Title

UTE bi-component analysis of T2* relaxation in articular cartilage

Journal

Osteoarthritis and Cartilage, 24(2)

ISSN

1063-4584

Authors

Shao, H
Chang, EY
Pauli, C
et al.

Publication Date

2016-02-01

DOI

10.1016/j.joca.2015.08.017

Peer reviewed

HHS Public Access

Author manuscript

Osteoarthritis Cartilage. Author manuscript; available in PMC 2017 February 01.

Published in final edited form as:

Osteoarthritis Cartilage. 2016 February ; 24(2): 364–373. doi:10.1016/j.joca.2015.08.017.

UTE bi-component analysis of T2* relaxation in articular cartilage

H. Shao[†,‡], **E.Y. Chang**[‡,§], **C. Pauli**[‖], **S. Zanganeh**[‡], **W. Bae**[‡], **C.B. Chung**[‡,§], **G. Tang**[†,*], and **J. Du**[‡,*]

[†]Department of Radiology, Shanghai Tenth People's Hospital, Tongji University School of Medicine, Shanghai 200072, China

[‡]Department of Radiology, University of California, San Diego, San Diego, CA 92103, USA

[§]Radiology Service, VA San Diego Healthcare System, San Diego, CA 92161, USA

[‖]Department of Molecular and Experimental Medicine, The Scripps Research Institute, LA Jolla, CA, USA

SUMMARY

Objectives—To determine T2* relaxation in articular cartilage using ultrashort echo time (UTE) imaging and bi-component analysis, with an emphasis on the deep radial and calcified cartilage.

Methods—Ten patellar samples were imaged using two-dimensional (2D) UTE and Car-Purcell-Meiboom-Gill (CPMG) sequences. UTE images were fitted with a bi-component model to calculate T2* and relative fractions. CPMG images were fitted with a single-component model to calculate T2. The high signal line above the subchondral bone was regarded as the deep radial and calcified cartilage. Depth and orientation dependence of T2*, fraction and T2 were analyzed with histopathology and polarized light microscopy (PLM), confirming normal regions of articular cartilage. An interleaved multi-echo UTE acquisition scheme was proposed for *in vivo* applications ($n = 5$).

Results—The short T2* values remained relatively constant across the cartilage depth while the long T2* values and long T2* fractions tended to increase from subchondral bone to the superficial cartilage. Long T2*s and T2s showed significant magic angle effect for all layers of cartilage from the medial to lateral facets, while the short T2* values and T2* fractions are insensitive to the magic angle effect. The deep radial and calcified cartilage showed a mean short T2* of 0.80 ± 0.05 ms and short T2* fraction of 39.93 ± 3.05% *in vitro*, and a mean short T2* of 0.93 ± 0.58 ms and short T2* fraction of 35.03 ± 4.09% *in vivo*.

[*]Address correspondence and reprint requests to: J. Du, University of California, San Diego, Department of Radiology, 200 West Arbor Drive, San Diego, CA 92103-8756, USA. Tel: 1-(619)-543-3512; Fax: 1-(619)-543-3736. G. Tang, Department of Radiology, Shanghai Tenth People's Hospital, Tongji University School of Medicine, Shanghai 200072, China. Tel: 86-(21)-66306242; Fax: 86-(21)-66306242. jiangdu@ucsd.edu (J. Du).

Author contributions

HS, EYC, CP, SZ, WB, GT, CBC, and JD designed research; HS, SZ, and JD performed research; HS, and JD analyzed data; HS, EYC, SZ, WB, GT, CBC, and JD wrote the paper.

Conflict of interest

The authors of this work have no conflicts of interest to report relevant to this work.

Conclusion—UTE bi-component analysis can characterize the short and long T2* values and fractions across the cartilage depth, including the deep radial and calcified cartilage. The short T2* values and T2* fractions are magic angle insensitive.

Keywords

UTE; T2*; Bi-component analysis; Deep radial and calcified cartilage

Introduction

Articular cartilage is a highly ordered tissue that can be functionally and structurally divided into the superficial, middle, deep, and calcified cartilage layers[1]. By exploiting the intrinsic magnetic resonance (MR) properties of cartilage, current techniques allow for the non-invasive assessment of many of the structural components. As a result, MR imaging has emerged as the modality of choice for evaluating articular cartilage injury and repair. Although MR imaging has been proven effective in the morphologic evaluation of knee articular cartilage, with reported sensitivities of 93–94% for the detection of surface irregularity and/or loss of cartilage thickness[2–5], the calcified cartilage has been virtually unexplored with conventional MR imaging. This region of cartilage may be critically important, since micro-cracking and vascular invasion of the calcified cartilage have been implicated in the pathogenesis of osteoarthrosis[6,7]. Unfortunately, conventional clinical pulse sequences are unable to acquire signal from this structure. Due to the high mineral content, the calcified cartilage has intrinsically short T2* characteristics with estimated T2* values of 1.0–3.3 ms[8]. The ability to image and quantify the calcified cartilage may be useful for detection of compromise in early osteoarthrosis or to follow longitudinal changes that accompany repair procedures.

With the advent of ultrashort echo time (UTE) MR imaging, species with predominantly short $T2^*$ properties can be interrogated in a non-invasive fashion[9–12]. However, it is still challenging to image and quantify the calcified cartilage even with UTE sequences, mainly because it is thin (a relatively constant percent of the total articular cartilage thickness at approximately 5%) and subject to partial volume effects[13]. We have previously proposed a dual adiabatic inversion recovery preparation scheme to invert and null long $T2^*$ signals from the more superficial layers of articular cartilage and marrow fat, which allows for imaging of the calcified cartilage[14]. Another approach is to use multi-component analysis to quantify both the short and long $T2^*$ components[15–18]. Multi-component analysis has been successfully applied to the articular cartilage[8,15], cortical bone[16], meniscus[17], and tendons[18] to quantify their T2*s and relative fractions of short and long $T2^*$ components using whole-body clinical MR scanners.

The calcified cartilage is well suited for evaluation using multi-component analysis due to its short T2* value and potential for separation from adjacent long $T2^*$ signals. However, the deep radial and calcified cartilage layers remain difficult to separate due to partial volume and susceptibility effects and from this point forward, in our manuscript, are considered together. The purpose of this study was to determine both short and long T2* relaxation times and their relative fractions across the whole cartilage thickness, with an emphasis on

the deep radial and calcified cartilage in cadaveric patella samples. *In vivo* assessment of short and long T2*s and relative fractions across the femorotibial cartilage in healthy volunteers was also performed using UTE imaging techniques with bi-component analyses at 3.0 T.

Materials and methods

Patella samples

Ten fresh patellae from cadaveric knees of ten donors (9 males, 1 female, age range = 48–58 years, mean ± standard deviation of 54.8 ± 5.5 years) were obtained from our institutional morgue. Surrounding soft tissues were removed. A transverse slab of ~5 mm thickness was cut and stored in a phosphate buffered saline (PBS) soaked gauze at 4°C prior to MR imaging.

MR imaging

Imaging of cadaveric patellae was performed on a GE 3T Signa TwinSpeed MR scanner (GE Healthcare Technologies, Milwaukee, MI) with maximum peak gradient amplitude of 40 mT/m, and slew rate of 150 mT/m/s. The only hardware modification implemented on the scanner was the addition of a specialized transmit-receive (T/R) switch, which enabled the receiver pre-amplifiers to be switched much more rapidly after the end of the RF transmitted pulse. The 2D UTE sequence employed a specially designed radio-frequency (RF) “half”-excitation pulse together with a variable rate selective excitation (VERSE) technique to synchronize RF excitation and gradient ramp-down[19]. The combination of VERSE and radial ramp sampling enabled very short delay time between the RF excitation and free induction decay (FID) data acquisition. By using the fast T/R switch, the delay time, or echo time was reduced to 8 μs[11]. The 2D UTE pulse sequence employed a radial ramp sampling and thus was subject to eddy currents[20]. The gradient anisotropy and eddy currents of our 3T scanner were minimized through gradient calibration. Timing for slice selection gradients and readout gradients was manually tuned. Artifacts originating from these errors were further reduced by empirically shifting the radial k-space trajectories during on-line image reconstruction. Further, a hysteresis gradient was added after each readout gradient[21]. This reset pulse results in residual magnetization that is less dependent on the preceding waveform history and results in more consistent gradient errors that can be corrected through k-space trajectory shift.

A 1-inch T/R birdcage coil was used for signal excitation and reception. The patellae samples were placed in perfluorooctyl bromide (PFOB) solution to minimize susceptibility effects at tissue-air junctions. The sample was placed into the iso-center of the MR scanner. The relationship between the patellae samples and B_0 is shown in Fig. 1. The imaging protocol included a 2D UTE sequence, a conventional 2D spoiled gradient recalled echo (SPGR) sequence, a T1-weighted fast spin echo (FSE) sequence and a Car-Purcell-Meiboom-Gill (CPMG) sequence. A centrally placed single slice was imaged. Typical UTE imaging parameters included: repetition time (TR) = 200 ms, field of view (FOV) = 5 cm, readout = 512, number of projections = 455, reconstruction matrix = 512×512, acquired in-plane pixel size = 0.1 × 0.1 mm^2, slice thickness = 1.7 mm, 12 TEs (0.008, 0.1, 0.2, 0.4, 0.6,

0.8, 3, 5, 10, 20, 40 and 80 ms), 3 min per image. 2D SPGR, FSE and CPMG T2 acquisitions were performed with the same spatial resolution.

Tissue processing

Following MRI, the patellae samples were immediately fixed in Z-Fix (Anatech, Battle Creek, MI) for three days and then decalcified in TBD-2 (Thermo). The center of each sample was marked with a tissue marking dye (Cancer Diagnostics, Morrisville, NC) on the lateral and medial edges to provide orientation. Transverse sections covering the cartilage and subchondral bone were obtained after full decalcification, dehydration with alcohol, propar clearant (Anatech) and infiltration with paraffin (Paraplast, McCormick Scientific, Richmond, IL). Each tissue block was then trimmed on a microtome using the orientation marks for reference. 5 μm sections were cut at the defined central location to match the MRI scans, and stained with Safranin O-Fast Green for histopathology.

Histopathology

Safranin O-Fast Green stained slides were scanned with a Leica SCN4000 slide scanner (Buffalo Grove, IL) and viewed with Slide-Path software. Approximately 4–6 regions of interest (ROIs) per patella were chosen for histopathological analysis. A Mankin score ranging from 0 to 14 was assigned to each ROI by a musculosketal histopathologist (C.P., with 8 years of experience with a primary focus on articular cartilage)[22]. Each score was converted to a grade as follows: G1 = 0–2, G2 = 3–5, G3 = 6–9, G4 = 10–14. Grade 1 represented normal tissue, Grade 2 mild, Grade 3 moderate and Grade 4 severe degeneration. Considering the limited number of patellae, only normal tissue ROIs were selected for UTE bi-component analysis.

Polarized light microscopy (PLM)

PLM was performed with the Picrosirius Red stained sections centered on a rotating stage of an Olympus BX60 microscope (Shinjuku, Tokyo, Japan). Each sample was placed between a polarizer, a 546-Nanometer Interference Filter, a senarmont compensator and an analyzer, with the polarizer and analyzer orthogonally aligned to each other. Polarized light was used to transilluminate the sample. Polarized light was scattered by the sample, then traveled through the analyzer and was detected by a calibrated charge-coupled device (CCD) camera (Macrofire Optronics, Goleta, CA), generating PLM images. The same ROIs used for histopathologic Mankin grading were qualitatively assessed using the grading scale (grade 0–4) published by Vaudey to describe the birefringence characteristics of the articular cartilage matrix[23].

In vivo evaluation

Five healthy volunteers (all male, age range = 28–59 years, mean ± standard deviation of 40.4 ± 12.1 years) were used for *in vivo* evaluation after approval by our Institutional Review Board and written informed consent. An 8-channel, transmit-receive knee coil was used with interleaved multi-echo UTE acquisition scheme for fast T2* bi-component analysis of the femorotibial cartilage, including the deep radial and calcified cartilage. In this protocol four sets of four-echo UTE acquisitions with fat suppression were performed with

the following imaging parameters: FOV = 14 cm, TR = 200 ms, a single sagittal slice, slice thickness = 3 mm, flip angle = 45°, readout = 320, number of projections = 455, reconstruction matrix = 512×512, four sets of TEs (0.008/4.4/20/40 ms; 0.4/6.6/25/50 ms; 0.8/11/30/60 ms; 2.2/16/35/70 ms), a total scan time of 12 min. A single slice was used to minimize magnetization transfer (MT) effect associated with 2D multi-slice imaging.

Post processing and image analysis

The analysis algorithm was written in Matlab (The MathWorks Inc., Natick, MA, USA) and was executed offiine on the DICOM axial images obtained by the protocols described above. The program allowed placement of ROIs on the first UTE MR image of the series, which was then copied onto each of the subsequent images. The mean intensity within each of the ROIs was used for subsequent curve fitting. A previously reported bi-component exponential fitting model was used to fit the UTE T2* images[16,17]. This model fits only three parameters, including the short T2*, the long T2*, and the short or long T2* fraction. Noise is estimated automatically using a maximum likelihood estimation (MLE) algorithm. As a result, the bi-component fitting model can reliably estimate T2*s and fractions of the two components with a fitting error of less than 3% using data with a clinically achievable signal-to-noise ratio (SNR) of 50[17]. SNR was measured for the first echo image of each patella and was calculated as the ratio of the mean signal intensity inside the ROI to the standard deviation of the signal in an ROI placed in the background.

For specimen studies only ROIs in normal regions as verified by the histologic and PLM gold standards were used for quantitative analysis. As the deep radial and calcified cartilage is of subvoxel dimension, the placement of manual ROIs is susceptible to volume averaging and misregistration. Small linear ROIs each containing approximately 5–10 pixels were chosen to minimize this error. Small linear ROIs were also chosen for the subchondral bone. Above the deep radial and calcified cartilage, three regions including the superficial layer (20% of the depth), the middle layer (50% of the depth) and the radial layer (30% of the depth) were drawn for analysis. A global ROI covering the whole cartilage depth was used for quantitative analysis. A series of linear ROIs across the whole cartilage depth covering the subchondral bone to the articular surface were also analyzed to assess the depth dependence of UTE bi-component analysis. ROIs were also drawn for different layers across the whole cartilage from the medial to the lateral facets to investigate the magic angle effect. The same ROI analysis was also performed on the CPMG T2 data for comparison.

Compared with *in vitro* studies, the region definition for *in vivo* studies is less accurate and more challenging due to much lower spatial resolution. ROIs were drawn for the deep radial and calcified cartilage (a linear ROI above the subchondral bone), the radial cartilage (1/3 of the depth), the middle cartilage (1/3 of the depth) and the superficial cartilage (1/3 of the depth). Due to the fact that the deep radial and calcified cartilage was depicted better for the femoral cartilage compared with the tibial cartilage, only the femoral cartilage was analyzed for all *in vivo* studies.

Goodness of fit statistics including the R-squared value and standard error or fitting confidence level were calculated for both cadaveric human patellae and *in vivo* knee joint studies. Fit curves along with their 95% confidence intervals (CI) and residual signal curves

were created. For the *in vitro* study, 95% CI for short T2*, long T2*, short fraction and long fraction were calculated for the global ROI, the superficial layer, middle layer, radial layer, deep radial and calcified layer and subchondral bone of patellar cartilage. For the *in vivo* study, 95% CI for short T2*, long T2*, short fraction and long fraction were calculated for the global ROI, the superficial layer, middle layer, radial layer, deep radial and calcified layer of femoral cartilage.

Results

Fig. 1 shows clinical and UTE MR images as well as histology and PLM of a representative patella slice. Clinical sequences do not allow identification of the deep radial and calcified cartilage, while the corresponding UTE subtraction image (the first image with a TE of 8 μs minus the image with a TE of 3 ms) shows the normal appearance of the deep radial and calcified cartilage as a linear, well-defined high signal line adjacent to the low signal intensity subchondral bone. Histology of the human patellar specimen demonstrated normal articular cartilage with a Mankin score of 0–1. PLM analysis shows a Vaudey score of 0, further confirming that this patella is normal.

Fig. 2 shows representative UTE and CPMG images of the same patella sample shown in Fig. 1, as well as bi-component UTE T2* analysis and single-component CPMG T2 analysis of the subchondral bone (UTE T2* only), the deep radial and calcified cartilage (UTE T2* only), the deep layer, the middle layer, the superficial layer and a global ROI. The patella cartilage was depicted with a high SNR of 141.6 ± 16.1, which is much higher than the required SNR of 50 to reduce fitting errors down to less than 3% using UTE bi-component analysis. A relatively constant short T2* value of around 0.61–0.76 ms was observed for all the layers while the long T2* values ranged from 18 to 56 ms. The short T2* fraction decreased from 32.4% for the deep radial and calcified cartilage to 16.2% for the superficial layers. The subchondral bone shows a high short T2* fraction of 55.3%. In comparison, T2 decreased monotonically from 72 ms for the superficial layer to 44 ms for the middle layer, and 29 ms for the deep radial and calcified layer.

Fig. 3 shows UTE and CPMG images as well as histology and PLM of another patella slice. Histology confirmed this patella sample was normal with a Mankin score of 0–1. PLM also confirmed this patella sample was normal with a Vaudey score of 0. A high SNR of 130.5 ± 23.2 was observed for the patella cartilage, enabling robust UTE bi-component analysis in which linear ROIs covering from the subchondral bone to the superficial cartilage were drawn. Depth profiles of short and long T2*s as well as their relative fractions were plotted. Fitting standard errors were also shown. As is shown, the short T2* values remained relatively constant at 0.6–0.8 ms, while the short T2* fraction decreased monotonically from 33% for the deep radial and calcified cartilage to 18% for the superficial cartilage. The long T2* values increased from ~20 ms for the deep radial and calcified cartilage to ~60 ms for the superficial cartilage. T2 profile is very similar to the long T2* profile, both monotonically increasing from deep cartilage to superficial cartilage.

Fig. 4 shows the magic angle effect for UTE bi-component analysis of the normal patella sample shown in Fig. 3. The short T2* values as well as short and long T2* fractions are

insensitive to the magic angle effect, as evidenced by the small variation (less than ~30%) for all cartilage layers from the medial to the lateral facets. However, the long T2* values show obvious magic angle effect, as evidenced by the two peaks corresponding to collagen fibers orienting to ~54° relative to the B_0 field, where the long T2* values vary by more than ~300%. Fig. 5 shows the magic angle effect for CPMG single-component analysis of T2 of the same normal patella sample. Obvious magic angle effect was observed for all three layers, with T2 values varying by more than ~200%.

Table I shows a summary of the UTE bi-component and CPMG single component analyses of ten patellae. Mean and 95% CI of T2 and the short and long T2* values as well as their relative fractions in normal regions were shown for subchondral bone, the deep radial and calcified layer, the radial layer, the middle layer, the superficial layer and a global ROI covering all the layers mentioned above. On average the deep radial and calcified cartilage has a short T2* of 0.80 ± 0.03 ms and short fraction of 39.93 ± 1.89%, as well as a long T2* of 20.64 ± 0.95 ms and long fraction of 60.07 ± 1.89%. The short T2* values are relatively constant ranging from 0.65 to 0.83 ms across the whole cartilage thickness. The long T2* values increased from 21.42 ± 2.95 ms for the subchondral bone to 57.09 ± 1.85 ms for the middle layer and 50.97 ± 2.36 ms for the superficial cartilage. The short fraction decreased from 39.93 ± 1.89% for the deep radial and calcified cartilage to 18.00 ± 1.07% for the superficial cartilage. Meanwhile, T2 increased from 55.5 ± 1.48 ms for the radial layer to 85.72 ± 4.86 ms for the superficial cartilage.

Fig. 6 shows UTE T2* imaging of the knee of a normal volunteer. The four sets of four-echo UTE acquisitions covered both short and long T2* ranges. A SNR of 40.3 ± 3.8 was demonstrated, allowing relatively reliable estimation of short and long T2* components in the femorotibial cartilage. The deep radial and calcified cartilage and meniscus can be better depicted in the subtraction image [Fig. 6(K)] where a later echo image was subtracted from the first echo, thus effectively suppressing the more superficial layers of cartilage with longer $T2^*$s. The UTE images were assessed using bi-component analysis at ROIs drawn in the superficial, middle and radial layers as well as deep radial and calcified cartilage. These showed excellent curve-fitting, demonstrating a short T2* of 0.62 ± 0.20 ms (37.0% of the UTE signal) and a longer T2* of 23.59 ± 2.29 ms (63.0% of the UTE signal) for the deep radial and calcified cartilage. The short and longer T2* values for the superficial, middle and radial layers are largely consistent with the values from the specimens study.

The mean and 95% CI of T2* and fraction measurements from femoral cartilage, including the superficial layers, middle layer and deep radial and calcified cartilage of five healthy volunteers are listed in Table II. The deep radial and calcified cartilage has a mean short T2* of 0.93 ± 0.42 ms, long T2* of 29.57 ± 4.16 ms, and short fraction of 35.03 ± 3.59%, roughly consistent with those from the cadaveric patellar samples.

Discussion

It is challenging to image and quantify the calcified cartilage. First, the calcified cartilage has a short T2* relaxation time, requiring a short TE to detect the signal before complete decay. Second, although the calcified cartilage has a short mean T2* relaxation time, there is

the potential that small amounts of long T2* components exist, which may be inherent to healthy calcified cartilage tissue or arise with aging/pathologic changes. Third, the calcified cartilage has a small dimension with a thickness around 5% of the total cartilage thickness, requiring ultra-high spatial resolution for structure discrimination. Fourth, the calcified cartilage lies between the more superficial layers of cartilage and the subchondral bone, potentially rendering it vulnerable to susceptibility artifacts[24]. In our study, the small patella samples were placed within the aperture of a 1-inch birdcage coil at the iso-center of the magnet to minimize B_0 inhomogeneity. A high-order shimming was employed to further improve field inhomogeneity. Partial volume was minimized by using a small imaging FOV of 5 cm and a large acquisition matrix of 512×512, which resulted in a high in-plane spatial resolution of 0.1 × 0.1 mm^2. However, the relatively thick slice of 1.7 mm provided a significant partial volume effect along the slice direction.

The accuracy of UTE bi-component analysis has been previously validated through numerical simulation and phantom studies[16,17]. Our prior simulation results demonstrated that the bi-exponential fitting model accurately estimates $T2^*$ and relative fractions of the two components with a fitting error of less than 3% using data with a clinically achievable SNR of around 50[17]. In this study, a high SNR of ~140 was achieved for patella cartilage, suggesting accurate estimation of the short and long T2* components with fitting errors less than 2%. For the *in vivo* study, SNR for femoraltibial cartilage was around 40, resulting in less than 5% fitting error based on previous results from numerical simulations. T2* quantification is expected to be sensitive to eddy current effects, gradient timing errors and distortion, and field inhomogeneity[20]. These effects were minimized through manual adjustment of the delay times for each gradient and k-space shift during on-line image reconstruction. As a result, obvious bi-component behavior was demonstrated for all the cartilage layers in patellae including the deep radial and calcified cartilage *in vitro* (Fig. 2) and *in vivo* (Fig. 6).

Using bi-component fitting, we have demonstrated that the short T2* values remain relatively constant across the cartilage depth, while the long T2* values and long T2* fractions tend to increase from the calcified cartilage to the superficial cartilage. The increase in T2*/T2 across the cartilage depth is due to two factors: an increase in longer T2* values as well as an increase in longer T2* fractions. The deep radial and calcified cartilage is shown as a high signal line above the subchondral bone. This is likely due to T1 shortening, related to calcification-associated surface relaxation, similar to that seen in cortical bone[25]. Subchondral bone may be like cortical bone and have a short T1 and very low proton density[11]. The calcified cartilage may have a similar T1 to that of subchondral bone, but a higher proton density. While the superficial layers of cartilage may have higher proton densities but much longer T1s[26]. As a result, the deep radial and calcified cartilage show the highest signal because their T1s are shorter than those of the superficial layers of cartilage, and their proton densities are higher than those of the subchondral bone. Further analysis of T1 across the whole cartilage depth is needed to validate this hypothesis, and will be investigated in future studies.

We further demonstrate that the deep radial and calcified cartilage contains ~60% long T2* signal, likely from the longer T2* components in the deep radial and calcified cartilage, as

well as contamination from the adjacent superficial layers of cartilage due to confounding partial volume effects. It is technically challenging to separate them using 2D UTE imaging techniques, especially considering that the deep radial and calcified cartilage is a very thin layer with a thickness of ~100 μm or less[1]. The measured T2* relaxation times for the superficial layers were in the range of published values[15–17,27,28], indirectly validating our bi-component T2* quantification techniques. The superficial layers of cartilage contain about 15–20% signal from the short T2* tissues, likely due to water bound to proteoglycan (PG) and collagen[27,28]. A recent magnetization transfer study suggests three distinct water components in articular cartilage, including ~80% bulk water with a long T2 of 130–145 ms, ~3% water bound to PG with a short T2 of 8–12 ms, and ~12% water associated with collagen with a short T2 of 3–18 ms[29]. Meanwhile, multi-component T2 analysis of articular cartilage also suggests three distinct water pools with ~6% water bound to collagen, ~14% bound to proteoglycans (PG), and ~80% bulk water[27]. It is likely that the longer T2* component from the UTE bi-component analysis corresponds to bulk water, while the shorter T2* component corresponds to both PG bound water and collagen bound water. The PG and collagen bound water may have similar short T2* values, and thus present a technical challenge for their separation and quantification. For accurate estimation, a three-component model and much higher SNR may be required.

Obvious magic angle effect was observed for both the long T2* values from the UTE bi-component analysis and T2 from CPMG single-component analysis for all layers in normal patellae, as shown in Figs. 4 and 5. Individual variation as well as pathologic changes can cause variable T2* and T2 values. Studies have shown that abnormalities of calcified cartilage increase with advancing age[7]. In this study, only regions that were confirmed to be normal with histology and PLM were used for quantitative analysis. Aging effects were not investigated due to limited sample sizes. Therefore, variations in T2* and T2 are likely predominantly due to the magic angle effect. The radial and medial layers show stronger magic angle effects than the superficial layers, consistent with more parallel organized fibrils in the former and more randomly organized fibrils in the latter[30]. The different water pools in articular cartilage may have different angular dependent behaviors. The orientation at or near the magic angle can manipulate the exchange process between different pools of water molecules, hence changing the population characteristics for each pool of water molecules[31]. As a result, short and long T2* fractions vary as a function of the angular orientation of the specimen. However, variations in the short T2* values as well as short and long T2* fractions are less than 30%. This is significantly less than the ~300% variation in long T2* and 200–300% variation in T2. Therefore, the short T2* values as well as the short and long T2* fractions are much less sensitive to the magic angle effect, suggesting that they might be more robust biomarkers of cartilage degeneration.

More accurate T2* quantification of short T2* tissues relies on further optimization of the 2D UTE pulse sequences, mainly through the minimization of gradient distortions and eddy currents[20]. Another option is to use 3D UTE imaging together with bi-component analysis to quantify T2* of the deep radial and calcified cartilage. The 3D UTE sequences employ short rectangular pulses for excitation, minimizing eddy currents and partial volume artifacts[32]. The associated long scan time may be resolved by employing more advanced sampling strategies, such as acquisition-weighted stack of spirals (AWSOS)[15] and Cones

trajectories[33,34]. The combination of interleaved multi-echo 3D UTE data acquisitions and bi-component analysis may allow quantitative evaluation of the deep radial and calcified cartilage *in vivo*. However, the balance between scan times and image quality will need to be investigated in future studies. Any patient motion can have a large effect on the analysis of the thin layer of deep radial and calcified cartilage. Further research is needed to establish reliable 3D UTE bi-component analysis *in vivo*.

Furthermore, there are several different approaches to measure bound and free water fractions. Magnetization transfer imaging together with signal modeling provides bound and free water fractions together with their T1s and T2s[35,36]. Cross-relaxation imaging can also measure bound pool fraction, which shows moderate correlation with PG content[37]. It would be interesting to compare the short fractions derived from UTE bi-component analysis, MT modeling and cross-relaxation imaging.

In summary, our methods to measure T2* values in the deep radial and calcified cartilage *in vitro* and *in vivo* appear reproducible and provide values that are consistent with those predicted, though not previously proven, in the literature. These values hold great potential for providing a means to optimize pulse sequences in a tissue specific manner. T2* parameter mapping in the short T2* range may serve as an objective and quantitative means for the determination of tissue structural integrity and for lesion detection. Future research will include further optimization of the acquisition scheme, especially in the form of 3D UTE acquisitions to further reduce partial volume artifacts, as well as adaptation of these techniques for clinical use.

Acknowledgments

Funding source

The authors acknowledge grant support from GE Healthcare, NIH (1R01 AR062581-01A1 and 1R21 AR063894-01A1), and the VA Clinical Science Research and Development Service (Career Development Grant 1IK2CX000749) and the National Natural Science Foundation of China (81371517).

References

1. Bullough PG, Yawitz PS, Tafra L, Boskey AL. Topographical variations in the morphology and biochemistry of adult canine tibial plateau articular cartilage. J Orthop Res. 1985; 3:1–16. [PubMed: 3981289]
2. Bredella MA, Tirman PF, Peterfy CG, Zarlingo M, Feller JF, Bost FW, et al. Accuracy of T2-weighted fast spin-echo MR imaging with fat saturation in detecting cartilage defects in the knee: comparison with arthroscopy in 130 patients. AJR Am J Roentgenol. 1999; 172(4):1073–80. [PubMed: 10587150]
3. Disler DG, McCauley TR, Wirth CR, Fuchs MD. Detection of knee hyaline cartilage defects using fat-suppressed three-dimensional spoiled gradient-echo MR imaging: comparison with standard MR imaging and correlation with arthroscopy. AJR Am J Roentgenol. 1995; 165(2):377–82. [PubMed: 7618561]
4. Konig H, Sauter R, Deimling M, Vogt M. Cartilage disorders: comparison of spin-echo, CHESS, and FLASH sequence MR images. Radiology. 1987; 164(3):753–8. [PubMed: 3615875]
5. Recht MP, Piraino DW, Paletta GA, Schils JP, Belhobek GH. Accuracy of fat-suppressed three-dimensional spoiled gradient-echo FLASH MR imaging in the detection of patellofemoral articular cartilage abnormalities. Radiology. 1996; 198(1):209–12. [PubMed: 8539380]

6. Burr DB. Anatomy and physiology of the mineralized tissues: role in the pathogenesis of osteoarthrosis. Osteoarthritis Cartilage. 2004; 12(Suppl A):S20–30. [PubMed: 14698637]
7. Muir P, McCarthy J, Radtke CL, Markel MD, Santschi EM, Scollay MC, et al. Role of endochondral ossification of articular cartilage and functional adaptation of the subchondral plate in the development of fatigue microcracking of joints. Bone. 2006; 38:342–9. [PubMed: 16275175]
8. Du J, Carl M, Bae WC, Statum S, Chang E, Bydder GM, et al. Dual inversion recovery ultrashort echo time (DIR UTE) imaging and quantification of the zone of calcified cartilage. Osteoarthritis Cartilage. 2013; 21:77–85. [PubMed: 23025927]
9. Gold GE, Thedens DR, Pauly JM, Fechner KP, Bergman G, Beaulieu CF, et al. MR imaging of articular cartilage of the knee: new methods using ultrashort TEs. AJR Am J Roentgenol. 1998; 170:1223–6. [PubMed: 9574589]
10. Williams A, Qian Y, Bear D, Chu CR. Assessing degeneration of human articular cartilage with ultra-short echo time (UTE) T2* mapping. Osteoarthritis Cartilage. 2010; 18:539–46. [PubMed: 20170769]
11. Du J, Carl M, Bydder M, Takahashi A, Chung CB, Bydder GM. Qualitative and quantitative ultrashort echo time (UTE) imaging of cortical bone. J Magn Reson. 2010; 207:304–11. [PubMed: 20980179]
12. Williams A, Qian Y, Golla S, Chu CR. UTE-T2* mapping detects sub-clinical meniscus injury after anterior cruciate ligament tear. Osteoarthritis Cartilage. 2012; 20:486–94. [PubMed: 22306000]
13. Oegema T, Carpenter R, Hofmeister F, Thompson R. The interaction of the zone of calcified cartilage and subchondral bone in osteoarthritis. Microsc Res Tech. 1997; 37:324–32. [PubMed: 9185154]
14. Du J, Takahashi A, Bae WC, Chung CB, Bydder GM. Dual inversion recovery, ultrashort echo time (DIR UTE) imaging: creating high contrast for short-T2 species. Magn Reson Med. 2010; 63:447–55. [PubMed: 20099332]
15. Qian Y, Williams A, Chu CR, Boada FE. Multi-component T2* mapping of knee cartilage: technical feasibility ex vivo. Magn Reson Med. 2010; 64:1426–31. [PubMed: 20865752]
16. Diaz E, Chung CB, Bae WC, Statum S, Znamirowski R, Bydder GM, et al. Ultrashort echo time spectroscopic imaging (UTESI): an efficient method for quantifying bound and free water. NMR Biomed. 2012; 25:161–8. [PubMed: 21766381]
17. Du J, Diaz E, Carl M, Bae W, Chung C, Bydder GM. Ultrashort echo time imaging with bicomponent analysis. Magn Reson Med. 2012; 67:645–9. [PubMed: 22034242]
18. Juras V, Apprich S, Szomolanyi P, Bieri O, Deligianni X, Trattnig S. Bi-exponential T2* analysis of healthy and diseased Achilles tendons: an in vivo preliminary magnetic resonance study and correlation with clinical score. Eur Radiol. 2013; 23:2814–22. [PubMed: 23760303]
19. Conolly S, Nishimura D, Macovski A, Glover G. Variable-rate selective excitation. J Magn Reson. 1988; 78:440–58.
20. Wansapura JP, Daniel BL, Pauly J, Butts K. Temperature mapping of frozen tissues using eddy current compensated half excitation RF pulses. Magn Reson Med. 2001; 46:985–92. [PubMed: 11675651]
21. King, KF.; Gai, N.; Ganin, A.; Glover, GH. Correction for gradient amplifier hysteresis artifacts in spiral scans. Proceedings of the 8th Annual Meeting of ISMRM; Denver, USA. 2000. p. 336
22. Mankin HJ. Biochemical and metabolic aspects of osteoarthritis. Orthop Clin North Am. 1971; 2:19–31. [PubMed: 4940528]
23. Vaudey ED, Ghosh S, Ries M, Majumdar S. T2 relaxation time measurements in osteoarthritis. Magn Reson Imaging. 2004; 22:673–82. [PubMed: 15172061]
24. Eckstein F, Burstein D, Link TM. Quantitative MRI of cartilage and bone: degenerative changes in osteoarthritis. NMR Biomed. 2006; 19:822–54. [PubMed: 17075958]
25. Fantazzini P, Brown RJS, Borgia GC. Bone tissue and porous media: common features and differences studied with NMR relaxation. Magn Reson Imaging. 2003; 21:227–34. [PubMed: 12850712]
26. Gold GE, Han E, Stainsby J, Wright G, Brittain J, Beaulieu C. Musculoskeletal MRI at 3. 0 T: relaxation times and image contrast. AJR. 2004; 183:343–51. [PubMed: 15269023]

27. Reiter DA, Li PC, Fishbein KW, Spencer RG. Multicomponent T2 relaxation analysis in cartilage. Magn Reson Med. 2009; 61:803–9. [PubMed: 19189393]
28. Pauli C, Bae WC, Lee M, Lotz M, Bydder GM, Lima DD, et al. Radiology. 2012; 264:484–93. [PubMed: 22653187]
29. Lattanzio PJ, Marshall KW, Damyanovich AZ, Peemoeller H. Macromolecule and water magnetization exchange modeling in articular cartilage. Magn Reson Med. 2000; 44:840–51. [PubMed: 11108620]
30. Gründer W. MRI assessment of cartilage ultrastructure. NMR Biomed. 2006; 19:855–76. [PubMed: 17075962]
31. Wang N, Xia Y. Anisotropic analysis of multi-component T2 and T1rho relaxations in Achilles tendon by NMR spectroscopy and miscroscopic MRI. J Magn Reson Imaging. 2013; 38:625–33. [PubMed: 23349070]
32. Rahmer J, Bornert P, Groen J, Bos C. Three-dimensional radial ultrashort echo-time imaging with T2 adapted sampling. Magn Reson Med. 2006; 55:1075–82. [PubMed: 16538604]
33. Gurney PT, Hargreaves BA, Nishimura DG. Design and analysis of a practical 3D cones trajectory. Magn Reson Med. 2006; 55:575–82. [PubMed: 16450366]
34. Carl, M.; Du, J.; Azeverenyi, N.; Statum, S.; Chung, C.; Bydder, G. Imaging of the red and white zone of the meniscus usig a 3D Cones (UTE) subtraction pulse sequence. Proceedings of the 22nd Annual Meeting of ISMRM; Milan, Italy. 2014. p. 3997
35. Ramani A, Dalton C, Miller DH, Tofts PS, Barker GJ. Precise estimation of fundamental in-vivo MT parameters in human brain in clinically feasible times. Magn Reson Imaging. 2002; 20:721–31. [PubMed: 12591568]
36. Hodgson RJ, Evans R, Wright P, Grainger AJ, O'Connor PJ, Helliwell P, et al. Quantitative magnetization transfer ultrashort echo time imaging of the Achilles tendon. Magn Reson Med. 2011; 65:1372–6. [PubMed: 21500263]
37. Stikov N, Keenan KE, Pauly JM, Smith RL, Dougherty RF, Gold GE. Cross-relaxation imaging of human articular cartilage. Magn Reson Med. 2011; 66:725–34. [PubMed: 21416504]

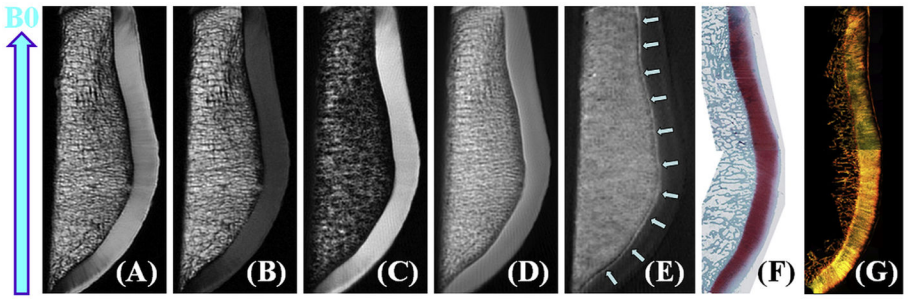

Fig. 1.

High resolution imaging of a cadaveric human patella from the knee joint of a 58-year old male donor with 2D PD-FSE (A), T1-FSE (B), SPGR (C), UTE (D), UTE with echo subtraction (E) and histology (F) as well as PLM (G). Clinical FSE and SPGR sequences show near zero signal for the deep radial and calcified cartilage, which is depicted as a high signal line above the subchondral bone (D and E). Histology and PLM confirmed this patella to be normal with a Mankin score of 0–1 and Vaudey score of 0. B_0 field (arrow) is shown for the experimental setup.

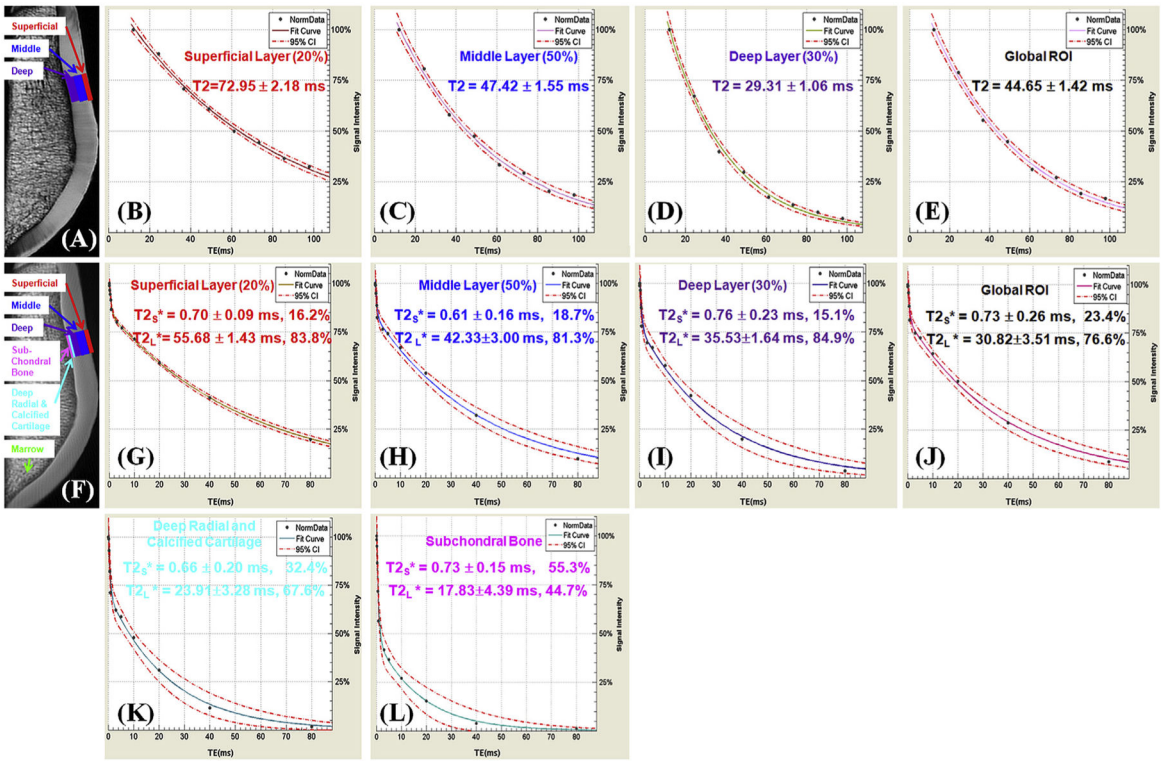

Fig. 2.

Single-component fitting of CPMG images of a normal patella specimen (A) with signal from ROIs drawn in the superficial (B), middle (C) and deep layers (D), and a global ROI (E), and bi-component fitting of UTE images of the same patella specimen (F) with signal from the same ROIs (G–J) as well as linear ROIs in the deep radial and calcified cartilage (K) and subchondral bone (L). T2 curves (B–E) show a single-component decay behavior with a T2 of 72.95 ms for the superficial layer (B), 47.42 ms for the middle layer (C) and 29.31 ms for the deep layer (D), and 44.65 ms for the global ROI (E). In (G–L) there is an obvious short T^*_2 component with a T^*_2 of 0.70 for the superficial layer (G), 0.61 ms for the middle layer (H), 0.76 ms for the deep layer (I), and 0.73 ms for the global ROI including all three layers (J). Furthermore, a short T2* of 0.66 ms was observed for the deep radial and calcified layer (K) and 0.73 ms for the subchondral bone (L). Long T2* components with T2*s of 55.68 (G), 42.33 (H), 35.53 (I), 30.83 (J), 23.91 (K), 17.83 (L) ms were also observed for the respective ROIs. Bound water fractions account for 23.4% for the global ROI (J),16.2% of the superficial layer (G), 18.7% for the middle layer (H), 15.1% for the deep layer (I), 32.4% for the deep radial and calcified cartilage (K) and 55.3% for the subchondral bone (L). 95% fitting confidence level was displayed for each fitting with $n = 8$ for CPMG T2 analysis and $n = 12$ for UTE T2* bi-component analysis. Fitting errors in single component T2 analysis and bi-component T2* analysis were also displayed.

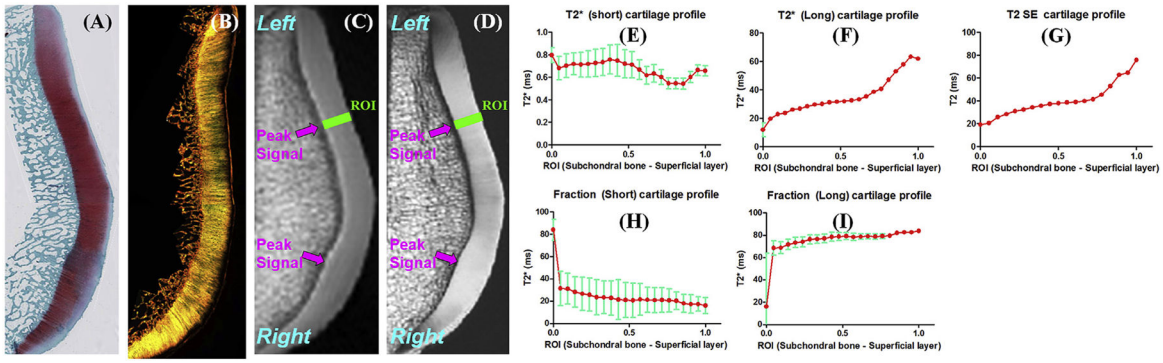

Fig. 3.

Safranin-O (A), PLM (B), UTE (C) and PD-SE (D) images of another normal patella sample from a 58-year old male donor. Line profiles for the short T2* (E), long T2* (F), short fraction (H), and long fraction (I) as well as CPMG T2 (G) are displayed. There is a gradual increase in long T2*, long fraction and T2 from the deep cartilage to the superficial cartilage. Fitting errors in single component T2 analysis and bi-component T2* analysis were displayed. Areas of peak signal corresponding to magic angle on the UTE and SE images were also depicted (arrows).

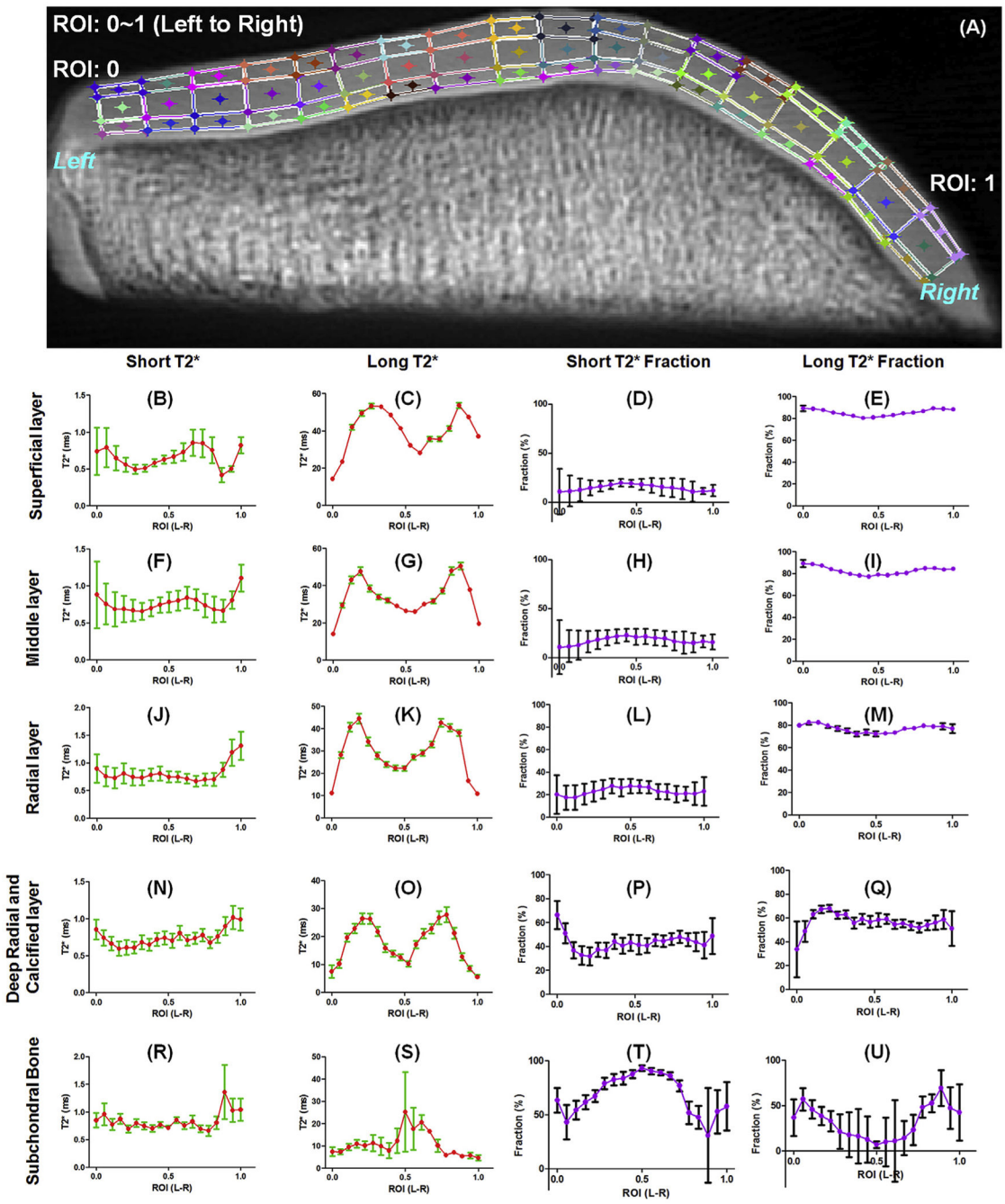

Fig. 4.

Magic angle study of a patella sample which was divided into different layers across the cartilage depth and different regions from left to right (A). UTE T2* bi-component analysis was performed to show the orientation dependence of short T2*, long T2*, short T2* fraction and long T2* fraction for the superficial layer (B–E), middle layer (F–I), radial layer (J–M), deep radial and calcified layer (N–Q) and subchondral bone (R–U), respectively. Significant magic angle effect was observed for long T2* values. The short and long T2*

fractions are relatively insensitive to the magic angle effect. Fitting errors in bi-component T2* analysis were displayed.

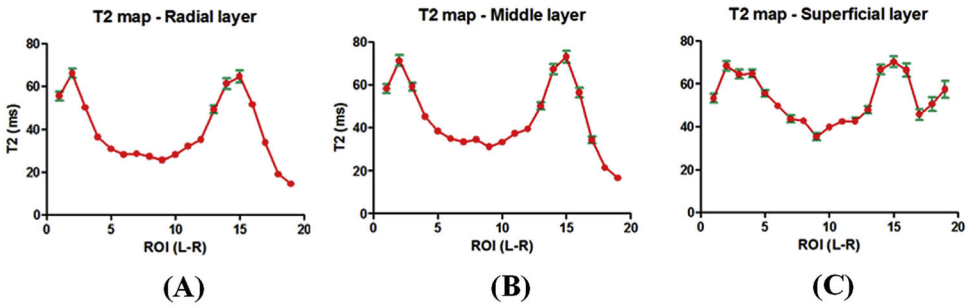

Fig. 5.

Magic angle study of CPMG T2 for radial layer (A), middle layer (B) and superficial layer (C) are displayed for ROIs drawn from the lateral to medial facets. Significant magic angle effect was observed for T2 values in all articular cartilage layers. Fitting errors in single component T2 analysis were displayed.

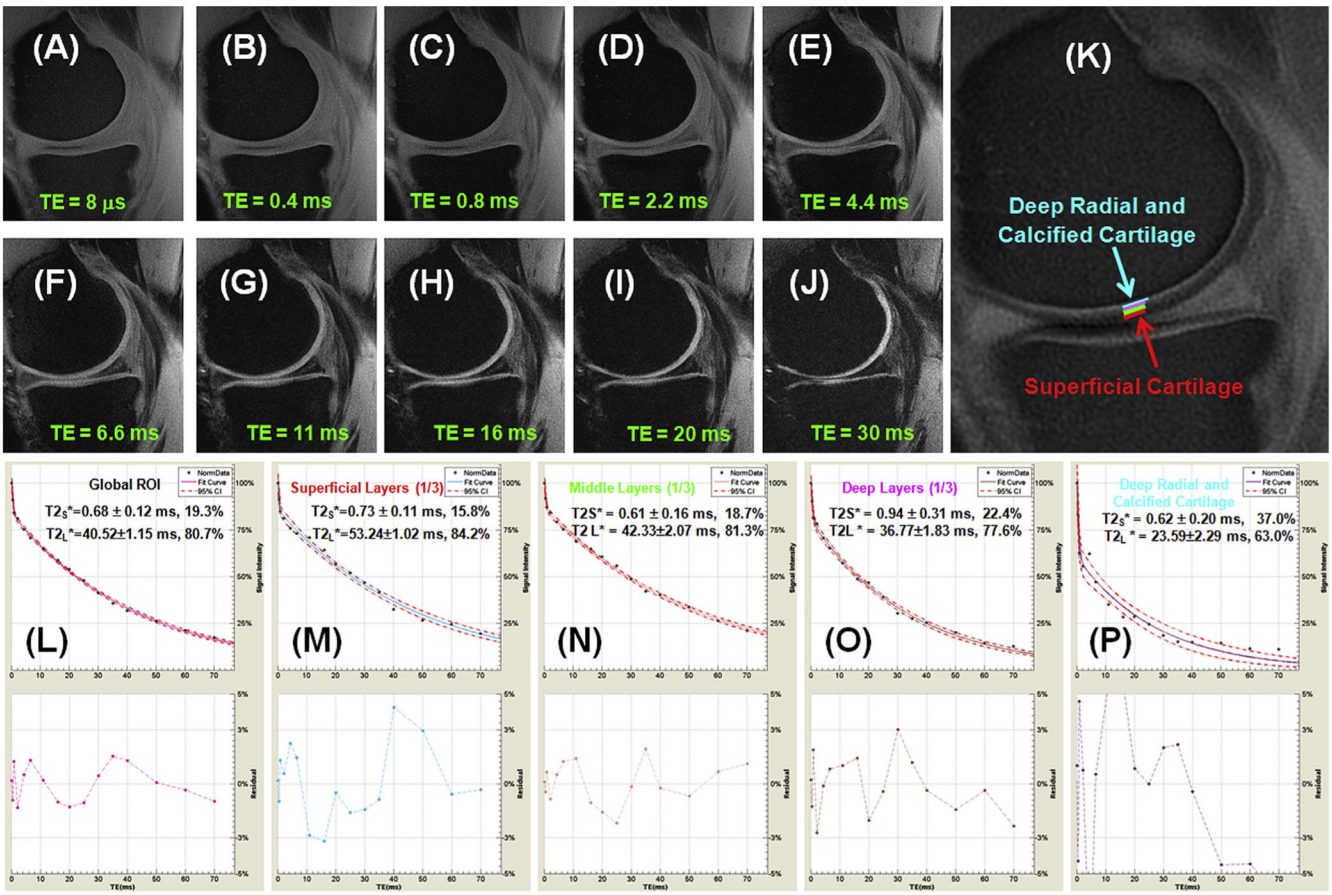

Fig. 6.

UTE imaging of a 59 year old volunteer who is a regular runner and in good health. Selected interleaved 4-echo UTE acquisitions with a TE of 8 μs (A), 0.4 ms (B), 0.8 ms (C), 2.2 ms (D), 4.4 ms (E), 6.6 ms (F), 11 ms (G), 16 ms (H), 20 ms (I), 30 ms (J), echo subtraction (K), and bi-component T2* analysis for the global ROI (L), superficial layer (M), middle layer (N), deep layer (O) and deep radial and calcified cartilage (P). The echo subtraction image was generated by subtracting the image with a TE of 2.2 ms from the first image with a TE of 8 μs. ROIs for the different layers of femoral cartilage were shown in (K). 95% fitting confidence level was displayed UTE T2* bi-component analysis with $n = 16$.

Table I

UTE bi-component analysis of 10 patellar samples ($n = 10$). Mean and 95% CI of the short and long T2*s and relative fractions are measured for subchondral bone, the deep radial and calcified layers, radial layer, middle layer, superficial layer and a global ROI involving all the layers. CPMG T2 analysis was also shown for comparison

Patella cartilage layers *in vitro*	**Short T2* (ms)**	**Long T2* (ms)**	**Short fraction (%)**	**Long fraction (%)**	**T2**
Subchondral bone	0.83 ± 0.03	21.42 ± 2.95	78.69 ± 1.96	21.31 ± 1.96	/
Deep radial and calcified layer	0.80 ± 0.03	20.64 ± 0.95	39.93 ± 1.89	60.07 ± 1.89	/
Radial layer (30%)	0.81 ± 0.03	44.96 ± 2.00	26.94 ± 1.80	73.06 ± 1.80	55.50 ± 1.48
Middle layer (50%)	0.72 ± 0.03	57.09 ± 1.85	20.41 ± 1.18	79.59 ± 1.18	75.99 ± 2.52
Superficial layer (20%)	0.65 ± 0.04	50.97 ± 2.36	18.00 ± 1.07	82.00 ± 1.07	85.72 ± 4.86
Global ROI	0.74 ± 0.03	51.84 ± 1.50	21.64 ± 1.31	78.36 ± 1.31	71.74 ± 1.97

Table II

UTE bi-component analysis of the femoral cartilage in the knee of 5 healthy volunteers ($n = 5$). Mean and 95% CI of the short and long T2*s and relative fractions are measured for the deep radial and calcified layers, radial layer, middle layer, superficial layer and a global ROI involving all the layers

Femoral cartilage layers *in vivo*	**Short T2* (ms)**	**Long T2* (ms)**	**Short fraction (%)**	**Long fraction (%)**
Deep radial and calcified layer	0.93 ± 0.42	29.57 ± 4.16	35.03 ± 3.59	64.97 ± 3.59
Radial layer (1/3)	1.34 ± 0.41	35.43 ± 5.64	30.36 ± 4.63	69.64 ± 4.63
Middle laser (1/3)	0.84 ± 0.21	55.50 ± 4.40	23.20 ± 6.13	76.80 ± 6.13
Superficial layer (1/3)	0.89 ± 0.15	51.45 ± 4.63	21.77 ± 5.30	78.23 ± 5.30
Global ROI	0.87 ± 0.18	46.80 ± 3.35	23.73 ± 6.01	76.27 ± 6.01